doi:10.1093/brain/awv045 BRAIN 2015: 138; 1613–1628 | 1613

BRAIN
A JOURNAL OF NEUROLOGY

PI3K/AKT pathway mutations cause a spectrum of brain malformations from megalencephaly to focal cortical dysplasia

Laura A. Jansen,[1,2] Ghayda M. Mirzaa,[2,3] Gisele E. Ishak,[4] Brian J. O'Roak,[5,6] Joseph B. Hiatt,[5] William H. Roden,[2] Sonya A. Gunter,[1] Susan L. Christian,[2] Sarah Collins,[2] Carissa Adams,[2] Jean-Baptiste Rivière,[2,7] Judith St-Onge,[2,7] Jeffrey G. Ojemann,[8] Jay Shendure,[5] Robert F. Hevner[2,8] and William B. Dobyns[2,3]

See Crino (doi:10.1093/brain/awv098) for a scientific commentary on this article.

Malformations of cortical development containing dysplastic neuronal and glial elements, including hemimegalencephaly and focal cortical dysplasia, are common causes of intractable paediatric epilepsy. In this study we performed multiplex targeted sequencing of 10 genes in the PI3K/AKT pathway on brain tissue from 33 children who underwent surgical resection of dysplastic cortex for the treatment of intractable epilepsy. Sequencing results were correlated with clinical, imaging, pathological and immunohistological phenotypes. We identified mosaic activating mutations in *PIK3CA* and *AKT3* in this cohort, including cancer-associated hotspot *PIK3CA* mutations in dysplastic megalencephaly, hemimegalencephaly, and focal cortical dysplasia type IIa. In addition, a germline *PTEN* mutation was identified in a male with hemimegalencephaly but no peripheral manifestations of the PTEN hamartoma tumour syndrome. A spectrum of clinical, imaging and pathological abnormalities was found in this cohort. While patients with more severe brain imaging abnormalities and systemic manifestations were more likely to have detected mutations, routine histopathological studies did not predict mutation status. In addition, elevated levels of phosphorylated S6 ribosomal protein were identified in both neurons and astrocytes of all hemimegalencephaly and focal cortical dysplasia type II specimens, regardless of the presence or absence of detected PI3K/AKT pathway mutations. In contrast, expression patterns of the T308 and S473 phosphorylated forms of AKT and *in vitro* AKT kinase activities discriminated between mutation-positive dysplasia cortex, mutation-negative dysplasia cortex, and non-dysplasia epilepsy cortex. Our findings identify PI3K/AKT pathway mutations as an important cause of epileptogenic brain malformations and establish megalencephaly, hemimegalencephaly, and focal cortical dysplasia as part of a single pathogenic spectrum.

1 University of Virginia, Neurology, Charlottesville, VA, USA
2 Seattle Children's Research Institute, Centre for Integrative Brain Research, Seattle, WA, USA
3 University of Washington, Paediatrics, Seattle, WA, USA
4 Seattle Children's Hospital, Radiology, Seattle, WA, USA
5 University of Washington, Genome Sciences, Seattle, WA, USA
6 Oregon Health and Science University, Molecular and Medical Genetics, Portland, OR, USA
7 Université de Bourgogne, Equipe Génétique des Anomalies du Développement, Dijon, France
8 University of Washington, Neurosurgery, Seattle, WA, USA

Correspondence to: Laura A. Jansen, MD PhD,
University of Virginia, Department of Neurology,
P.O. Box 801330, Charlottesville, VA 22908-1330 USA
E-mail: laura.jansen@virginia.edu

Received August 29, 2014. Revised December 12, 2014. Accepted December 22, 2014. Advance Access publication February 26, 2015

Keywords: malformations of cortical development; molecular genetics; childhood epilepsy; brain development

Abbreviations: CLOVES = congenital lipomatous overgrowth, vascular malformations, epidermal nevi and spinal/skeletal anomalies; DMEG = dysplastic megalencephaly; FCD = focal cortical dysplasia; HMEG = hemimegalencephaly; MEG = megalencephaly; mTOR = mammalian target of rapamycin; MIP = molecular inversion probe

Introduction

The PI3K/AKT/mTOR signalling pathway has been shown to be centrally important in both normal brain development and human neurological disease. Loss of function mutations in the tuberous sclerosis complex *TSC1* or *TSC2* genes, resulting in dysregulated mammalian target of rapamycin (mTOR) activity, are associated with brain lesions, epilepsy, cognitive impairment, and autism (European Chromosome 16 Tuberous Sclerosis Consortium, 1993; Slegtenhorst *et al.*, 1997). Loss of function mutations in phosphatase and tensin homologue (*PTEN*), resulting in dysregulated AKT activity, cause Cowden and Bannayan-Riley-Ruvalcaba syndromes (also known as PTEN hamartoma tumour syndrome), associated with megalencephaly (MEG), cognitive impairment, autism and epilepsy (Arch *et al.*, 1997; Liaw *et al.*, 1997; Pilarski *et al.*, 2013). Recently, we identified mosaic-activating mutations in *AKT3*, *PIK3CA*, which encodes the p110 catalytic subunit of phosphoinositide 3-kinase (PI3K), *PIK3R2*, which encodes the p85 regulatory subunit of PI3K, and *CCND2*, which encodes the AKT downstream target cyclin D2, in megalencephaly-capillary malformation syndrome and megalencephaly-polymicrogyria-polydactyly-hydrocephalus (MPPH) syndrome (Rivière *et al.*, 2012; Mirzaa *et al.*, 2014).

Mosaic *AKT3*, *PIK3CA* and *MTOR* mutations have been found in brain tissue resected from individuals with hemimegalencephaly (HMEG) (Lee *et al.*, 2012; Poduri *et al.*, 2012). The neuropathological phenotypes of tuberous sclerosis complex, *PTEN* mutation syndromes, and HMEG exhibit many similarities, including cortical dyslamination, cytomegaly and dysmorphic neurons (Huttenlocher and Wollmann, 1991; Richardson, 1991; Flores-Sarnat, 2002; Merks *et al.*, 2003). These histological characteristics are shared by focal cortical dysplasia (FCD), a condition causing the majority of intractable localization-related epilepsy in childhood (Blumcke *et al.*, 2011; Hauptman and Mathern, 2012). Activation of the PI3K/AKT pathway in FCD has been suggested by previous immunohistochemistry studies (Ljungberg *et al.*, 2006; Schick *et al.*, 2006, 2007).

We therefore performed next generation sequencing of brain tissue from a cohort of 33 children with either HMEG or FCD using molecular inversion probe (MIP) capture technology targeting 10 genes involved in the PI3K/AKT signalling pathway. Mutation status was correlated with clinical, imaging, pathological and immunohistological phenotype. In addition to identification of novel causative mutations, we demonstrate that mosaic mutation in a single gene, *PIK3CA*, can result in either MEG, HMEG, or FCD type IIa. Furthermore, increased PI3K/AKT/mTOR pathway signalling was evident in all type IIa and IIb FCD specimens in the absence of detected mutations, implicating other causative mechanisms leading to a common pathophysiology. These findings solidify MEG/HMEG/FCD as a single neurobiological spectrum disorder and suggest new potential therapeutic approaches.

Materials and methods

Paediatric cortical brain specimens

Specimens were collected from 33 children with intractable epilepsy due to HMEG or FCD who underwent resective surgery at Seattle Children's Hospital between 2004 and 2012. Four non-dysplasia epilepsy specimens with pathological diagnoses of gliosis were also examined. A control, non-epilepsy cortical specimen from a 4-year-old child was obtained during surgical approach for tumour resection. Informed consent for the use of a portion of the resected tissues for research purposes was obtained with the approval of the hospital's Institutional Review Board. Immediately after excision, the tissue was frozen in liquid nitrogen and stored at −80°C until use. Formalin-fixed, paraffin-embedded sections (4 μM) were prepared from tissue adjacent to each frozen specimen. The results of routine stains done for diagnostic purposes were reviewed and classified by R.F.H.

Multiplex targeted sequencing

Genomic DNA was isolated from 50–200 mg of frozen resected cortex using the Qiagen Gentra Puregene® Tissue kit. Targeted sequencing was performed using 12N (degenerate tag) single molecule MIP capture technology (Hiatt *et al.*, 2013). A pool of 350 single molecule MIP oligonucleotides targeting the coding sequences of 10 PI3K/AKT pathway genes was designed and optimized (*PIK3CA*, *PIK3CB*, *PIK3CD*, *PIK3R1*, *PIK3R2*, *PIK3R3*, *AKT1*, *AKT2*, *AKT3*, and *PTEN*). These upstream members of the PI3K/AKT pathway were chosen based on our previous findings in the megalencephaly syndromes megalencephaly-capillary malformation and MPPH (Rivière *et al.*, 2012). The MIPs tiled the coding exons and splice-junctions, a total of 12.6 kb of genomic sequence. Targeted capture was performed as previously described using 500 ng of DNA as template (O'Roak *et al.*, 2012). Following the post-capture PCR amplification, samples were subjected to massively parallel sequencing using the Illumina platform. Reads were mapped as described previously (O'Roak *et al.*, 2012). Read-pairs with identical tags (originating from the same capture event) were removed, leaving the read-pair with the highest estimated quality. We then identified all sites with at least two Phred-quality 30 non-reference

bases and compared the observed read counts to a site-specific empirical error model built from unrelated samples (binominal). Sites showing strong signal for mutation were evaluated for possible pathogenicity. The mean coverage of the target bases was 567×, with 86% of target bases at 50× coverage or greater and 92% of target bases at 10× coverage or greater. Full details regarding our single molecule MIP technology can be found in Hiatt *et al.* (2013).

Sanger sequencing

Standard Sanger sequencing was used to confirm all identified variants using custom intronic primers and standard PCR protocols (primer sequences available on request). Amplicons were Sanger sequenced at the Seattle BioMed Sequencing Core Facility. All mutations were tested in at least two independent amplification and sequencing reactions in the proband and available relatives. Sequence traces were analysed using Mutation Surveyor v3.97 (SoftGenetics).

Quantitative PCR

Quantitative PCR was performed using the Power SYBR® Green PCR Master Mix (Applied Biosystems) following the manufacturer's protocol. Three independent primer pairs across the *AKT3* gene were used to check for copy number variation. Primer sequences are available on request. Quantitative PCR was performed on an ABI 7900 HT real-time PCR system (Applied Biosystems) in a 384-well format using SDS 2.3 software. Each sample was analysed in triplicate in a total reaction volume of 10 µl using 20 ng of DNA. PCR conditions were 95°C, denaturation for 10 min, then 40 cycles each of 95°C for 15 s and 60°C for 1 min. Data analysis was carried out with RQ manager 1.2 using the ΔΔCT method to obtain the relative quantity values after normalizing with two reference genes (*ALB*, *RPP30*). Primers were designed using Primer3 (http://frodo.wi.mit.edu/primer3/).

Western blot analysis

Frozen cortical tissue (100–200 mg) was separated from underlying white matter and homogenized in 5 mM Tris/HCl (pH 7.4) with 0.32 M sucrose. The homogenates were centrifuged at 3000*g* for 5 min at 4°C. The supernatant was then centrifuged at 40 000*g* for 1 h at 4°C to pellet the membrane fraction. Thirty micrograms of protein from the cytosolic fraction was electrophoretically separated and transferred to an Immobilon®-FL PVDF membrane (Millipore). The membrane was blocked with Odyssey Blocking Buffer (LI-COR Biosciences), incubated in primary antibodies overnight at 4°C, and then incubated in goat anti-rabbit or goat anti-mouse infrared dye-labelled secondary antibody (IRDye®, LI-COR) or HRP-conjugated secondary antibody (Bio-Rad) for 2 h at room temperature. Infrared fluorescence (Odyssey Infrared Imaging System, LI-COR) or chemiluminescence (Kodak Gel Logic 2200 imaging system) was used for signal detection. Primary antibodies used for western blotting included rabbit monoclonal phospho-Akt (Ser473) XP, rabbit monoclonal phospho-Akt (Thr308), and mouse monoclonal Akt3 (all from Cell Signaling Technology). Binding of mouse monoclonal antibodies against β-tubulin (Novus Biologicals) was used as a loading control. Each blot was repeated twice and the results averaged.

Immunohistochemistry

Specimens were deparaffinized by incubation in xylene, followed by rehydration through graded ethanol/water solutions and equilibration in PBS. Antigen retrieval was performed by heating in 0.01 M sodium citrate (pH 6.0) in a 90°C water bath for 45 min. Specimens were then blocked in PBS with 10% donkey serum, 0.1% Triton™ X-100 and 2% bovine serum albumin for 30 min and incubated overnight at 4°C in primary antibodies diluted in blocking solution. Primary antibodies used in these studies included mouse monoclonal MAP2 (Millipore), rabbit monoclonal phospho-Akt (Ser473) XP, rabbit monoclonal phospho-Akt (Thr308), and rabbit monoclonal phospho-S6 ribosomal protein (Ser235/246) XP (all from Cell Signaling Technology). Slides were then incubated in fluorescent secondary antibodies (Alexa Fluor®) at room temperature for 2 h. Following incubation in DAPI nuclear counterstain and Sudan Black to block endogenous fluorescence, sections were examined and photographed using a Zeiss Axio Imager Z1 or Nikon Eclipse Ni-U epifluorescence microscope. Maximal cell soma diameters of all neurons with combined MAP2 and phospho-S6 immunofluorescence were measured manually in at least five microsopic fields using Nikon NIS Elements software.

AKT kinase activity measurements

Frozen cortical brain tissue (50 to 300 mg) was separated from underlying white matter and homogenized in buffer containing (in mM) glycine 200, NaCl 150, EGTA 50, EDTA 50, and sucrose 300 (pH 9), plus 10 µl of protease inhibitor cocktail. Samples were centrifuged and protein concentrations determined in the supernatant using a Bradford protein assay. AKT kinase activity was measured using the Cell Signaling Technology assay kit (Cat. no. 9840). AKT was immunoprecipitated from 100 µg of extracted protein with bead-conjugated phospho-Akt (Ser473) rabbit monoclonal antibody. Precipitated AKT was then incubated with a GSK-3 fusion protein substrate and ATP in kinase buffer at 30°C for 2 h. GSK-3 fusion protein phosphorylation was detected and quantitated by western blotting using phospho-GSK-3α/β (Ser21/9) antibodies and infrared detection (Odyssey Li-Cor Imager). For each specimen the measured density of the phosphorylated GSK-3 fusion protein band was normalized to that of the anti-AKT IgG light chain (gel loading control) and expressed relative to the control surgical specimen.

Results

Cortical dysplasia cohort characteristics

Thirty-three children who underwent surgical resection for intractable epilepsy due to cortical dysplasia were studied, in addition to one child with imaging features of bilateral HMEG (termed dysplastic megalencephaly, DMEG). Males and females were equivalently represented (16 males,

18 females), as was the affected hemisphere in the unilateral cases (15 right, 17 left). Skin manifestations, including capillary malformations and epidermal nevi, were present in 6 of 34 (18%). The average patient age at the time of surgery was 6.5 years, with a range of 1 month to 14 years. Of the surgical cases, six had HMEG (hemispheric overgrowth and cortical dysplasia) and 27 had FCD: five with FCD I (cortical dyslamination without dysmorphic neurons), 13 with FCD IIa (dyslamination with dysmorphic neurons), six with FCD IIb (dyslamination with dysmorphic neurons and balloon cells) and three with FCD IId (dyslamination adjacent to lesions acquired early in life) (Blumcke *et al.*, 2011). Of the 27 FCD patients, nine had multilobar cortical dysplasia, and in the remaining 18 the area of dysplasia was localized to a single lobe (Supplementary Table 1).

MRI and histopathological findings

MRI images for all patients were reviewed by a single investigator (G.E.I.) and graded based on abnormalities of the cortex, underlying white matter, ventricular system, and extra axial space. Representative T_2-weighted images are shown in Fig. 1, while evaluation of all patients is detailed in Supplementary Table 2. As expected, the most severe findings in all categories were seen in the patients diagnosed with DMEG or HMEG, with 6/7 exhibiting severe abnormalities of the cortex (similar to hemispheric lissencephaly or polymicrogyria) and severe white matter dysplasia (manifested as increased T_2 and FLAIR signal, in some cases with cystic changes and calcifications). Also seen in the affected hemispheres were dilation of the lateral ventricle and enlargement of the extra axial space with prominent vasculature. In contrast, the majority of the patients with FCD type I and II (19/24) had mild to moderate cortical abnormalities, including localized undersulcation, cortical thickening, and/or blurring of the grey–white junction. Localized abnormalities in white matter signal were also frequent in FCD, present in 15/24. Ventricular and extra axial space enlargement was rare in the FCD patients. All FCD IIa and IIb patients had at least one abnormality evident on retrospective review of MRI images, whereas 2/5 FCD I patients were thought to have completely normal imaging studies (Supplementary Table 2).

The results of routine histopathological analysis were reviewed for all surgical specimens and classified based on the International League Against Epilepsy (ILAE) consensus classification (Blumcke *et al.*, 2011), as shown in Supplementary Table 3. All HMEG specimens in our cohort (6/6) demonstrated histopathological features of FCD type IIa, as indicated by the presence of cortical dyslamination, blurring of the grey–white junction, and dysmorphic neurons, but the absence of balloon cells. Other common histopathological features of HMEG cortex were calcifications (3/6), microscopic heterotopia (2/6), and areas of layer 1 (molecular layer) fusion, similar to that seen in polymicrogyria (4/6). Interestingly, aggregates of immature small diameter neurons were found at relatively high frequency in FCD IIa (5/13) but not FCD IIb (0/6), whereas layer 1 fusion was also found in some cases of FCD IIa (2/13) but not FCD IIb (0/6).

Identification of PI3K/AKT pathway mutations

We performed multiplex targeted sequencing of the *PIK3CA*, *PIK3CB*, *PIK3CD*, *PIK3R1*, *PIK3R2*, *PIK3R3*, *AKT1*, *AKT2*, *AKT3* and *PTEN* genes in genomic DNA isolated from frozen brain tissue resected from the 33 children with HMEG/FCD and intractable epilepsy. This sequencing identified pathogenic mutations in 4 of 33 patients (12%), in addition to the patient with DMEG and systemic features (buccal DNA). These patients are presented in detail below. In the remaining 29 HMEG/FCD patients, no pathogenic sequence variants were found. Full details regarding pathogenic mutations identified by sequencing are presented in Supplementary Table 4. Based on the report of Poduri *et al.* (2012), analysis for *AKT3* gene duplication by quantitative PCR was performed on samples from the three HMEG patients without identified mutations; this analysis was negative.

Patient LR12-033: mosaic PIK3CA mutation in a patient with DMEG, capillary malformations and segmental overgrowth

This female child had severe congenital megalencephaly associated with asymmetric enlargement of the face, dramatic overgrowth of both hands and both feet, extensive capillary malformations of the skin, and several epidermal nevi, features consistent with CLOVES syndrome (congenital lipomatous overgrowth, vascular malformations, epidermal nevi and spinal/skeletal anomalies; Kurek *et al.*, 2012). Her brain MRI, briefly described in an earlier report (Rivière *et al.*, 2012), showed diffuse cortical malformation resembling HMEG on both sides, ventriculomegaly, and white matter dysplasia with relative enlargement of the left hemisphere as compared with the right (Fig. 1A and Supplementary Table 2). Deep sequencing of genomic DNA isolated from a buccal swab identified a mosaic p.Glu545Lys *PIK3CA* mutation in 26% of reads, which was absent from blood (Table 1). This mutation was also detected by Sanger sequencing of buccal DNA. Given the bilateral severe cortical malformation, she was not considered a candidate for epilepsy surgery and brain tissue was therefore not available for analysis.

Patient LR12-241: mosaic PIK3CA mutations in a patient with HMEG and linear epidermal nevus

This male child developed focal-onset and myoclonic seizures within the first few days of life that became intractable to anticonvulsant medications. Linear epidermal nevi were identified on his right upper extremity, trunk, and face. Brain MRI revealed enlargement of the right occipital, parietal and posterior temporal lobes (Fig. 1B) with irregular

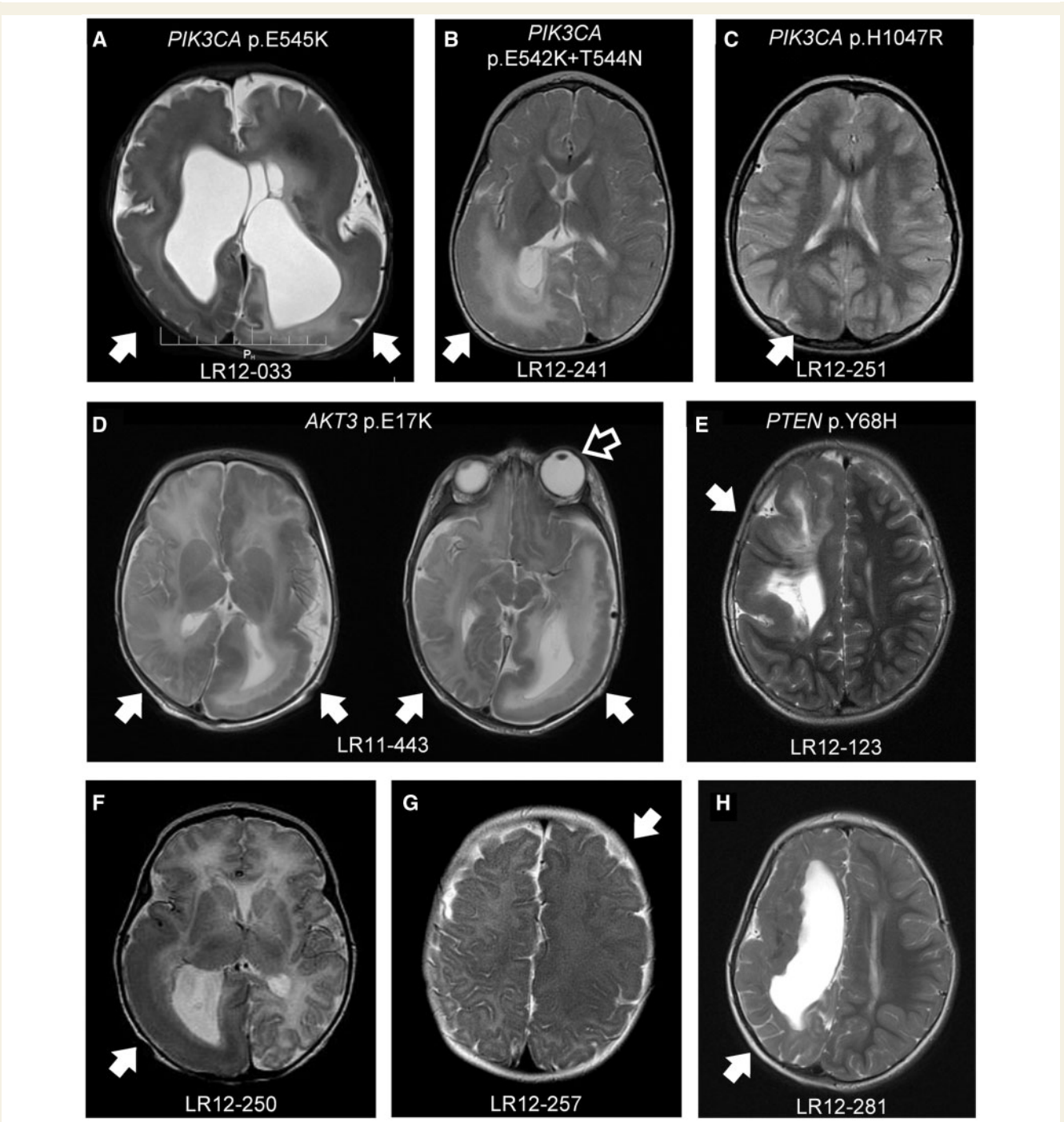

Figure 1 MRI findings in dysplastic brain malformations with and without detected mutations. T_2-weighted images are shown. Filled arrows indicate regions of abnormality, including ventricular enlargement, variable degrees of cortical dysmorphism (i.e. pachygyria, polymicrogyria, or undersulcation), periventricular nodular heterotopia, abnormal white matter signal, and/or widening of the extra-axial space. (**A**) DMEG; (**B**, **E–H**) HMEG; (**C**) FCD type IIa; (**D**) bihemispheric asymmetric dysplasia. The open arrow indicates unilateral ocular enlargement in Patient LR11-443, who exhibits severe abnormality of the left hemisphere (HMEG) along with milder abnormalities of the posterior portion of the right hemisphere.

cortex, undulation of the grey–white matter junction, and underlying dysplastic white matter (Supplementary Table 2). He underwent hemispherectomy at 17 months of age, which resulted in seizure freedom. Deep sequencing of genomic DNA isolated from the resected temporal lobe identified two mosaic mutations in *PIK3CA*: p.Glu542Lys and p.Thr544Asn (Table 1). Both were present in ~31% of reads and were confirmed by Sanger sequencing (Fig. 2A). Manual examination of the deep sequencing reads revealed these two mutations occurred on the same DNA strand, likely representing a single mutational event.

Table 1 Sequencing results

Subject	Age (years)	Sex	Diagnosis	Gene	Mutation	Type	Level and tissues tested	Sanger validation	Parental testing
LR12-033	1	F	DMEG	*PIK3CA*	p.Glu545Lys	Mosaic	26% (buccal) negative (blood)	Yes	n/a
LR12-241	1.4	M	HMEG	*PIK3CA*	p.Glu542Lys	Mosaic	31% (brain)	Yes	n/a
				PIK3CA	p.Thr544Asn	Mosaic	31% (brain)	Yes	n/a
LR12-251	5.3	F	FCD IIa	*PIK3CA*	p.His1047Arg	Mosaic	4.7% (brain)	Below detection level*	n/a
LR11-443	1	F	HMEG	*AKT3*	p.Glu17Lys	Mosaic	10-18% (brain) negative (dura, skin, fibroblast cx)	Yes	Negative
LR12-123	9.2	M	HMEG	*PTEN*	p.Tyr68His	Germline	50% (brain, blood, saliva)	Yes	Mother negative, father unavailable

*Validated on repeat single molecule MIP sequencing. n/a = not available.

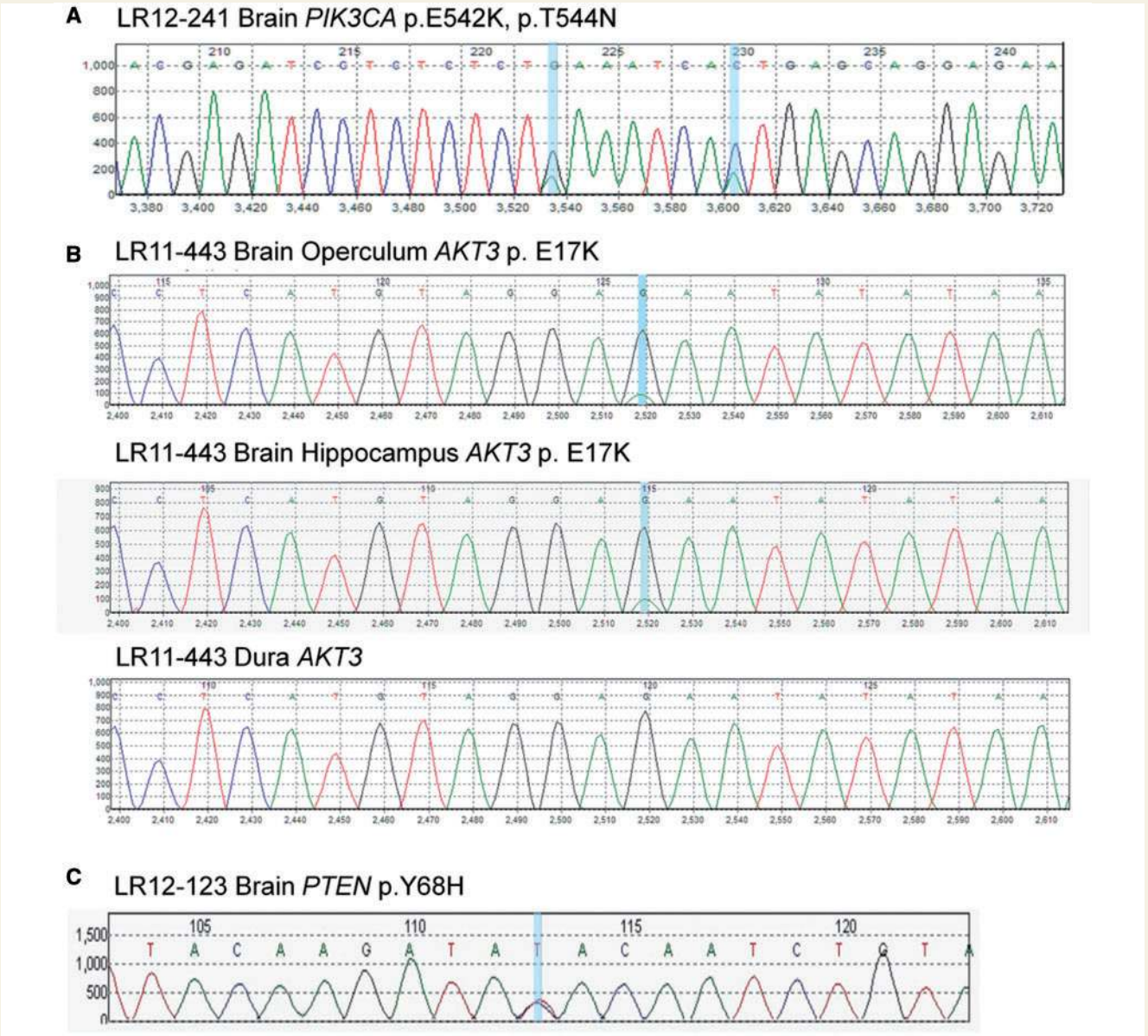

Figure 2 Sanger sequencing confirmation of mutations detected in HMEG brain by molecular inversion probe capture technology. Sequence changes are highlighted by the blue bars. (**A**) Mosaic *PIK3CA* p.E542K and p.T544N mutations from HMEG brain LR12-241. (**B**) Mosaic *AKT3* p.E17K mutation from HMEG brain LR11-443 operculum and hippocampus, which was absent in overlying dura. (**C**) Germline *PTEN* p.Y68H heterozygous mutation detected in LR12-123 brain.

Patient LR12-251: mosaic PIK3CA mutation in a patient with localized FCD IIa

This female child developed medically refractory epilepsy at 3 years of age and was found on MRI to have a localized area in the right occipital lobe of undersulcation, blurring of the grey–white matter junction, and underlying increased T_2 signal in the white matter (Fig. 1C and Supplementary Table 2). She was developmentally normal and had no extra-CNS lesions. She underwent right occipital resection at 5 years of age with resolution of her seizures. Histopathology was consistent with FCD IIa (Supplementary Table 3). Deep sequencing of resected cortical tissue identified a *PIK3CA* p.His1047Arg mutation in 4.7% of reads (Table 1). This level of mosaicism was undetectable by Sanger sequencing, but was confirmed on repeat single molecule MIP analysis.

Patient LR11-443: mosaic AKT3 mutation in a patient with HMEG, cutaneous vascular malformations and unilateral ocular enlargement

At birth, this female patient was found to have enlargement of the left eye and vascular skin lesions on her leg and back resembling cutis marmorata telangiectatica congenita. She developed seizures at 3 days of life. MRI demonstrated enlargement and dysplasia of the entire left cerebral hemisphere, including an undersulcated gyral pattern with pebbling of the grey-white matter junction and underlying dysplastic white matter, as well as more subtle abnormalities of the right hemisphere (Fig. 1D and Supplementary Table 2). Her epilepsy progressed to intractable clonic seizures and infantile spasms. She underwent a left hemispherectomy at 1 year of age. Deep sequencing of genomic DNA isolated from resected frontal, temporal, opercular, and hippocampal tissue identified a mosaic p.Glu17Lys *AKT3* mutation in 10–18% of reads (Table 1 and Supplementary Table 4). The presence of the mutation was also visible by Sanger sequencing (Fig. 2B), even though this level of mosaicism is traditionally below the level of Sanger sensitivity. The *AKT3* mutation was absent from dura overlying the area of resection (single molecule MIP analysis), as well as from epidermis and fibroblasts cultured from a biopsy of unaffected skin (Sanger sequencing).

Patient LR12-123: germline PTEN mutation in a patient with isolated HMEG

This male patient developed focal onset seizures shortly after birth which proved resistant to anticonvulsant therapies. Brain MRI revealed right frontal overgrowth with pachygyria and dysplastic underlying white matter and lateral ventricle (Fig. 1E and Supplementary Table 2). He underwent hemispherectomy at 9 years of age and became seizure-free. Deep sequencing of resected cortical tissue identified a germline *PTEN* p.Tyr68His mutation that was confirmed by Sanger sequencing (Fig. 2C) and was also present in peripheral blood (Table 1). The *PTEN* mutation was not present in his mother; DNA samples from his father were not available. No peripheral stigmata of the PTEN hamartoma tumour syndrome were found at the time of his most recent evaluation.

PI3K/AKT pathway activation in HMEG/FCD specimens with and without identified mutations

The activation state of kinases in the PI3K/AKT pathway can be examined through the use of antibodies specific for the phosphorylated forms of their target proteins. AKT is phosphorylated on Thr308 (or its equivalent) by PDPK1 (3-phosphoinositide dependent protein kinase 1) and on Ser473 by the mTORC2 complex (Fig. 7). Increased AKT T308 phosphorylation results from either activation of PI3K or PDPK1 or loss of activity of the inhibitory protein PTEN, while increased AKT S473 phosphorylation results from activation of mTOR. Phosphorylation of AKT at both sites is required for full kinase activity (Alessi *et al.*, 1996). In contrast, phosphorylation of ribosomal protein S6 serves as a downstream readout of activation at any level of the PI3K/AKT/mTOR pathway (Bellacosa *et al.*, 2005; Bhaskar and Hay, 2007; Manning and Cantley, 2007). In these experiments, we assayed the phosphorylation state of AKT and ribosomal protein S6 in 20 HMEG/FCD brain specimens by western blot and fluorescence immunohistochemistry analysis.

As shown in Fig. 3, nearly all HMEG and FCD specimens (19/20) exhibited an increase in both T308 and S473 pAKT expression in comparison to control cortex as measured by western blotting of cortical homogenates. While all HMEG specimens had elevated pAKT expression, the samples with the highest levels were those with identified *PIK3CA*, *AKT3*, and *PTEN* mutations (Fig. 3). Among the FCD IIa and FCD IIb specimens, a range of pAKT levels was found, from mildly to markedly elevated (Fig. 3B and C, and Supplementary Fig. 1). The level of pAKT in the FCD IIa specimen with the PIK3CA mutation was only mildly increased, likely reflecting the low level of mosaicism (4.7%) in this specimen. Interestingly, in non-dysplasia epilepsy cortex, S473 pAKT was elevated (suggestive of downstream pathway activation) whereas T308 pAKT was not (indicating lack of upstream pathway activation). Total AKT3 levels were similar among all samples (Fig. 3A and Supplementary Fig. 1).

The phosphorylation state of AKT and ribosomal protein S6 were next analysed in HMEG and FCD specimens by double label fluorescence immunohistochemistry to determine which cell types were affected by dysregulated PI3K/AKT pathway signalling. In each HMEG, FCD IIa and FCD IIb specimen analysed, prominent phospho-S6 expression was found in the cytoplasm of MAP2-positive neurons (Fig. 4). The proportion of affected neurons ranged from 10% to nearly 50% in samples both with and without identified PI3K/AKT pathway mutations. In the specimen with the germline *PTEN* mutation (which should be present as a single copy in all cells), only a small percentage

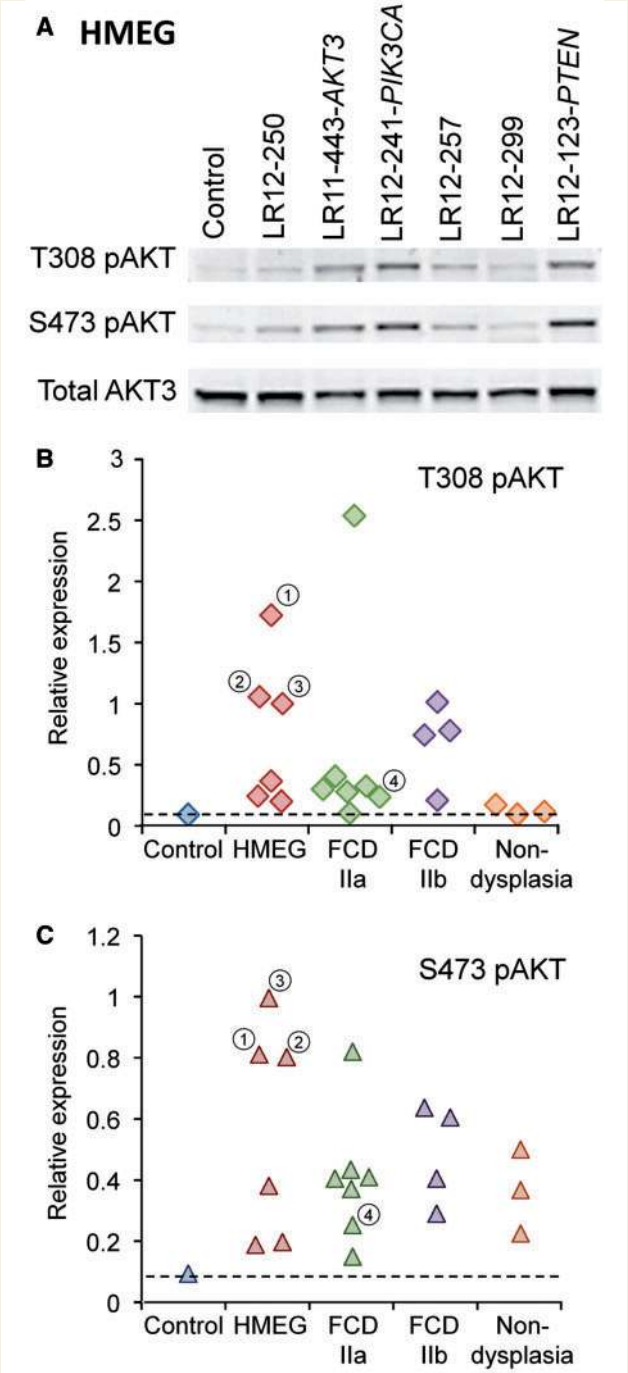

Figure 3 Western blot analysis of T308 pAKT, S473 pAKT, and total AKT3 levels in dysplastic brain specimens. (**A**) Representative western blot showing increased expression of T308 pAKT and S473 pAKT in six HMEG brain specimens as compared to control, non-epileptic brain (all surgical specimens). The highest levels of pAKT were seen in the HMEG specimens with detected *PIK3CA*, *AKT3* and *PTEN* mutations. (**B** and **C**) Summary of relative T308 pAKT (**B**) and S473 pAKT (**C**) levels in 17 dysplastic brain specimens (HMEG, FCD IIa, and FCD IIb) as compared with control brain and three non-dysplasia epilepsy brain specimens. The ratio of T308 pAKT or S473 pAKT band intensity to total AKT3 band intensity was determined for each specimen and is expressed relative to that of specimen LR12-241, which was run concurrently on each blot. [1]LR11-443 *AKT3* mutation; [2]LR12-123 *PTEN* mutation; [3]LR12-241 *PIK3CA* mutation; [4]LR12-251 *PIK3CA* mutation.

(~10%) of neurons exhibited increased phospho-S6 expression (Fig. 4D). This suggests that a second, unidentified somatic mutation may be required for excessive PI3K/AKT pathway activation, similar to what has been found in the tumours of Cowden syndrome (Bonneau and Longy, 2000). Our single molecule MIP sequencing data makes a mosaic intragenic mutation of *PTEN* unlikely, but a low level deletion has not been excluded. In FCD IIb specimens, phospho-S6 was present in both neurons and balloon cells (Fig. 4I). Astrocytic phospho-S6 immunofluorescence was visible in all HMEG/FCD specimens as well as in non-dysplasia epilepsy cortex (Fig. 4 and Supplementary Fig. 2A and B).

We observed that neuronal size seemed to vary substantially between different HMEG/FCD specimens (Fig. 4). Phospho-S6 positive neuronal diameter was therefore quantified in 12 HMEG/FCD specimens and compared with neuronal diameter measured in four control paediatric specimens (Supplementary Fig. 3). In all HMEG/FCD II samples, phospho-S6 immunofluorescence was present in neurons with enlarged diameters ($>25\,\mu M$) as well as in smaller neurons. The most striking neuronal hypertrophy was in the specimen with the *AKT3* p.Glu17Lys mutation (LR11-443) (Fig. 4C). Lesser hypertrophy of phospho-S6 positive neurons was seen in the two specimens with *PIK3CA* mutations (LR12-241 and LR12-251, Fig. 4A and B), whereas neurons in the specimen with the *PTEN* mutation were intermediate in size (Fig. 4D). This heterogeneity in phospho-S6 positive neuronal size extended to the mutation-negative HMEG and FCD specimens (Supplementary Fig. 3).

We next used fluorescence immunohistochemistry to determine which cell types exhibited evidence of upstream PI3K/AKT pathway activation in HMEG/FCD. T308 pAKT immunofluorescence was present in neuronal cytoplasm and nuclei in the HMEG/FCD specimens with identified *PIK3CA*, *AKT3* and *PTEN* mutations (Fig. 5). Neuronal T308 pAKT immunofluorescence was also present in many HMEG/FCD specimens without detected mutations, consistent with western blot results (Fig. 3 and Supplementary Fig. 4). Dysplastic specimens with and without detected mutations also exhibited T308 pAKT labelling in astrocytes (Supplementary Fig. 2). In contrast to T308 pAKT, in HMEG/FCD as well as non-dysplasia epilepsy specimens S473 pAKT expression was present in the neuronal soma, but not nucleus, and was also prominent in the cortical neuropil (Supplementary Fig. 5).

In addition to analysing the phosphorylation state of AKT at T308 and S473, we directly measured AKT kinase activity *in vitro* in cortical extracts. Marked increases in AKT kinase activity were found in specimens with AKT/PI3K pathway mutations as compared with control and non-dysplasia epilepsy brain (Fig. 6). Importantly, a substantial increase in AKT kinase activity was found for the FCD IIa specimen with the low-level mosaic *PIK3CA* p.His1047Arg mutation (LR12-251), even though pAKT

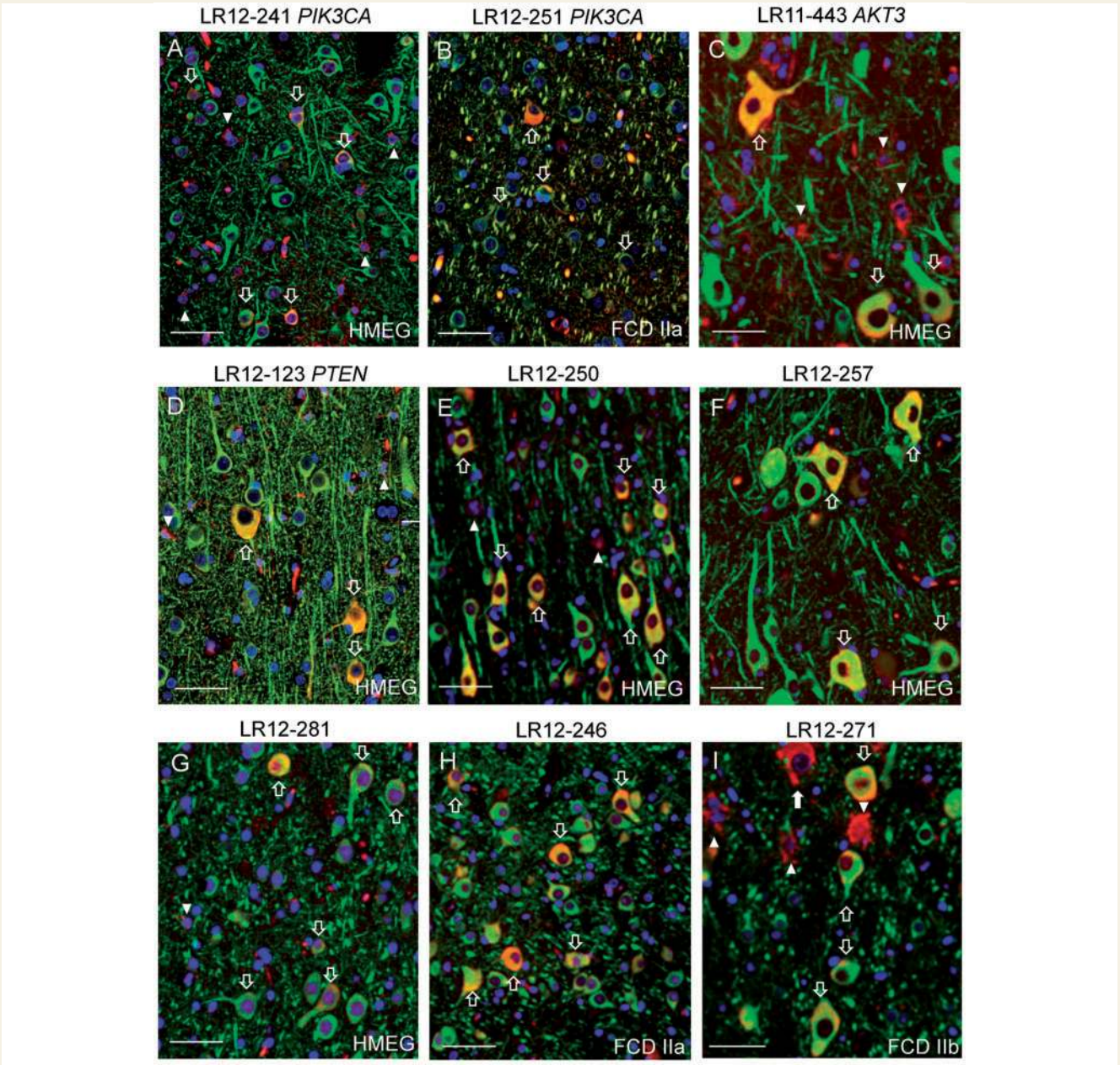

Figure 4 Phosphorylated ribosomal S6 protein (phospho-S6) immunofluorescence in neurons from dysplastic brain specimens with and without detected mutations. Red = phospho-S6; Green = neuronal marker MAP2; Blue = nuclear marker DAPI. Neurons co-localizing phospho-S6 and MAP2 appear orange-yellow in colour, and are indicated by the open arrows. Arrowheads indicate phospho-S6 positive cells with astrocytic morphology. The closed arrow in **I** indicates a phospho-S6 positive balloon cell in FCD IIb. Scale bars = 50 μm.

T308 and S473 levels in whole-tissue homogenates for this sample were only mildly elevated (Fig. 3).

Discussion

We report a detailed phenotypic study of 34 children with DMEG, HMEG or FCD and critical genetic information that expands our understanding of this spectrum of disorders. This is the first study of the cortical dysplasias that combines thorough review of imaging studies, massively parallel sequencing using single molecule MIP technology for detection of low levels of brain mosaicism, and examination of affected tissue by a combination of histopathology, immunohistochemistry, western blotting, and *in vitro* kinase assays. All of these data converge to demonstrate a shared pathogenesis for these developmental disorders.

Neuroimaging

In our surgical cohort, brain imaging studies demonstrated wide variation in distribution of cortical malformation

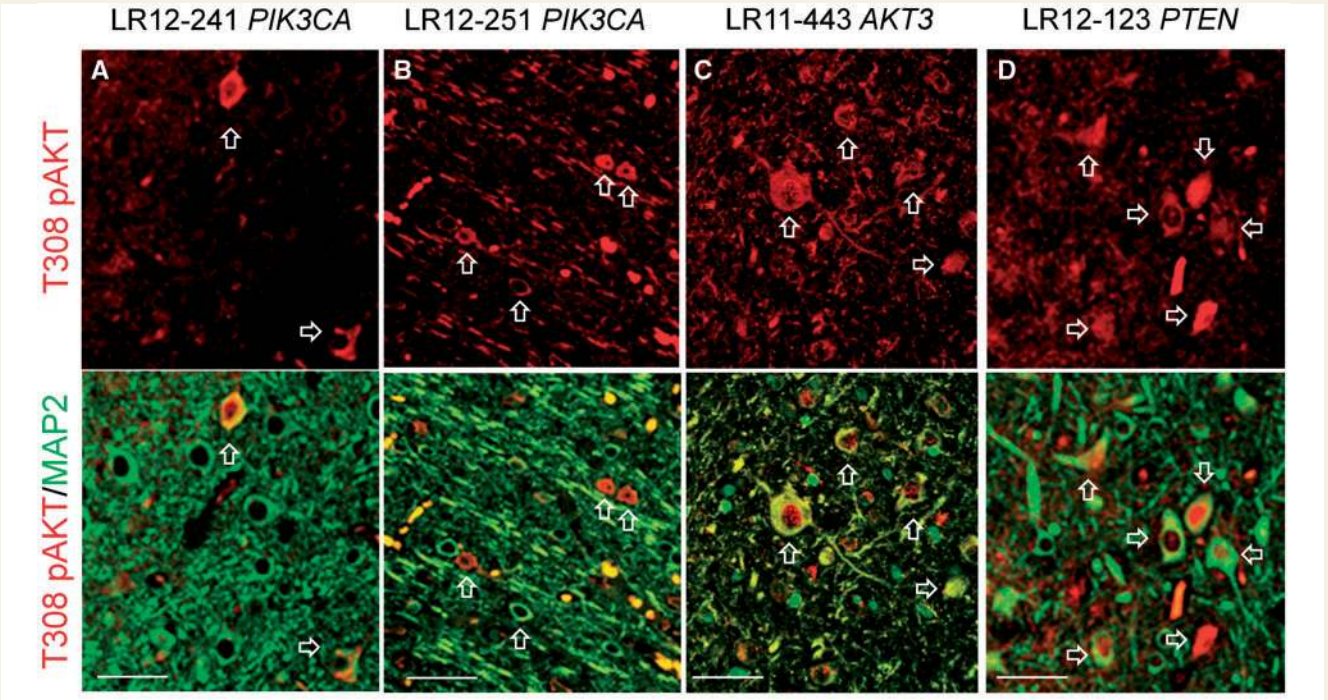

Figure 5 Neuronal T308 pAKT immunofluorescence in dysplastic brain specimens with PI3K/AKT pathway mutations. Red = T308 pAKT; Green = MAP2. Open arrows indicate neurons colocalizing T308 pAKT and MAP2. In many neurons T308 pAKT is visible in both the cytoplasm and nucleus. Scale bars = 50 μm.

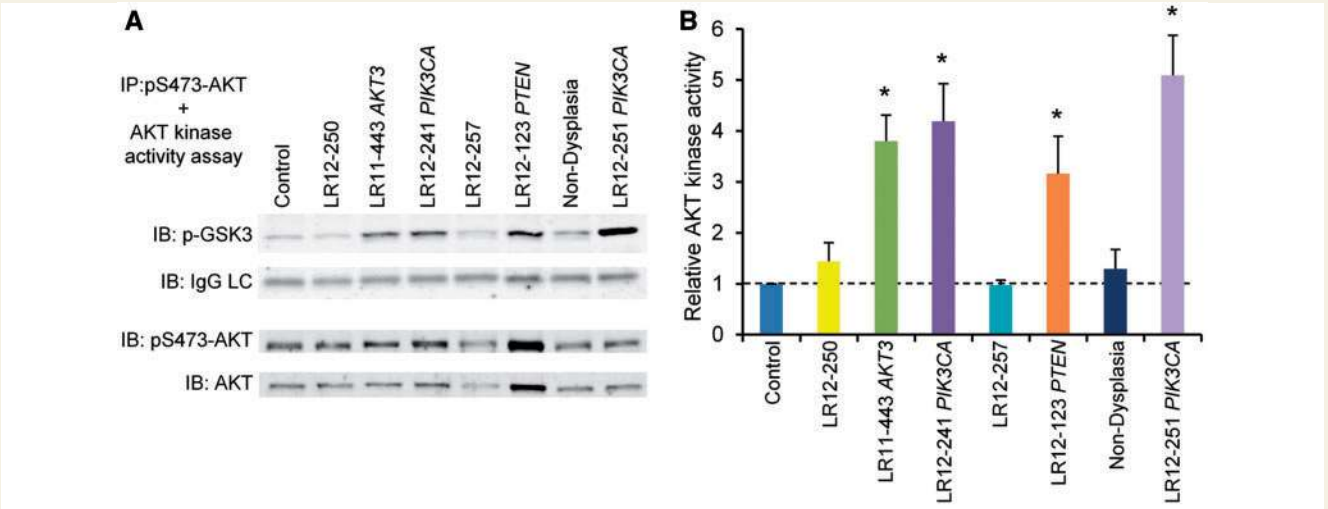

Figure 6 *In vitro* AKT kinase assay of frozen brain extracts showing highest levels of kinase activity in specimens with detected PI3K/AKT pathway mutations. (**A**) Representative western blot showing phosphorylated GSK 3 fusion protein (p-GSK3) levels after incubation with immunoprecipitated pAKT and ATP. IgG LC = IgG light chain from immunoprecipitating antibody, used for normalization of p-GSK3. (**B**) Average relative kinase activity ± SEM as determined from three to five separate blots per sample. Note that other than specimen LR12-123, AKT kinase activity is not correlated with pS473-AKT levels, consistent with a requirement for phosphorylation at both the S473 and T308 sites for full AKT kinase activity. *$P < 0.05$ versus control, one-way ANOVA followed by post-tests.

from lobar to multilobar to hemispheric, similar to published cohorts (Barkovich and Chuang, 1990; Nakahashi *et al.*, 2009; Colombo *et al.*, 2012). The involved areas usually demonstrate subtle irregularity of the pial surface, variably thick (5–15 mm) cortex with poor differentiation of the grey-white border, and shallow sulci. The underlying white matter appears abnormal. More severe malformations in our cohort were characterized by ventricular

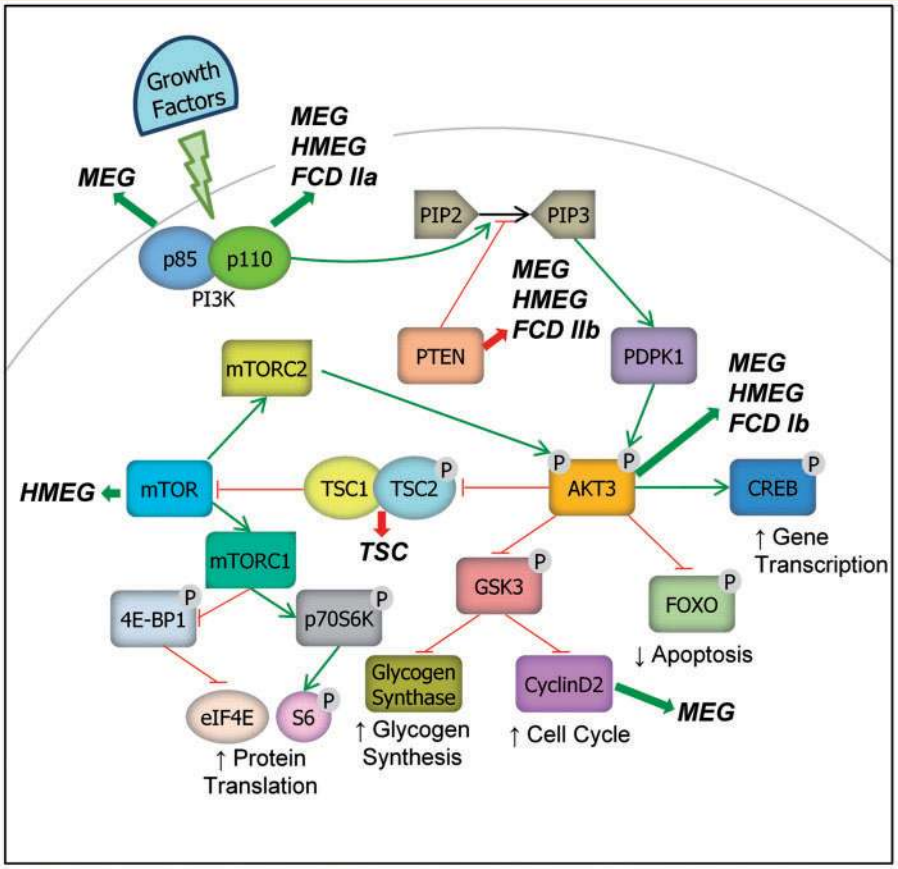

Figure 7 The PI3K/AKT kinase pathway and associated brain malformations. Wide green arrows indicate disorders caused by activating mutations, whereas wide red arrows indicate disorders caused by loss of function mutations. See text for references.

dilation, widened extra-axial spaces with enlarged dysplastic blood vessels, markedly thick (10–15 mm) cortex, visible white matter cysts, and variable enlargement of other brain structures such as the deep nuclei, brainstem and cerebellum. We also report imaging data on a female child with severe bilateral brain and extra-CNS involvement associated with a mosaic mutation of *PIK3CA* found in saliva-derived DNA, as we believe that this completes the spectrum of brain involvement of this class of cortical malformations. Rather than using the problematic term 'bilateral' HMEG, we classify her malformation as DMEG. Although rare, bilateral malformations of cortical development with features of HMEG or FCD have been reported (Jahan *et al.*, 1997; Fauser *et al.*, 2009; Kometani *et al.*, 2010).

Histopathology

Microscopic review of brain tissue demonstrated histopathological features of FCD I ($n = 5$), FCD IIa ($n = 19$), FCD IIb ($n = 6$), or FCD III ($n = 3$) in all 33 brains, as this was one of our inclusion criteria. The histology of the six children with HMEG as well as another 13 patients with more focal lesions was consistent with FCD IIa including loss of cortical lamination, dysmorphic neurons, and blurred grey–white matter junction with increased heterotopic neurons in white matter (Blumcke *et al.*, 2011). Six patients exhibited both dysmorphic neurons and balloon cells, consistent with FCD IIb. In our FCD IIa/IIb cohort, we also found several variable features including disparity in size of dysmorphic neurons and presence or absence of layer 1 fusion, calcifications, neuronal heterotopias and clusters of immature cells.

Sequencing

Our sequencing studies detected mutations in upstream components of the PI3K/AKT pathway in 4 of 19 patients with FCD type IIa histopathology (including three of six with HMEG and 1 of 13 with localized FCD IIa) and none of six with FCD IIb. No mutations were identified in the eight specimens with FCD types I or III. Combining our data with prior reports, brain DNA mutations of core PI3K/AKT/mTOR pathway components have now been found in 12 of 34 (35%) patients with HMEG including five with mutations of *PIK3CA*, five with mutations of *AKT3*, and one each with mutation of *PTEN* or *MTOR* (Lee *et al.*, 2012; Poduri *et al.*, 2012). All were mosaic

except for the *PTEN* mutation (which we discuss below), representing 8–40% of reads corresponding to 16–80% of cells, as the mutations are heterozygous. We also report the first patient with localized FCD (FCD IIa by pathology) and mosaic mutation of *PIK3CA*, although this result is not surprising given the similarities between FCD and HMEG on brain imaging, histopathology and immunohistochemistry. The level of mosaicism in the FCD specimen was only 4.7%, lower than any reported patients with HMEG. Although more data are needed to assess the relationship between phenotype and level of mosaicism, these data suggest that localized dysplasias (i.e. FCD) could be associated with lower levels of mosaicism than extensive dysplasias, due to the occurrence of somatic mutations later during brain development.

The sequencing panel used in our study, which focused on the upstream members of the PI3K/AKT pathway, was designed based on previous results from the megalencephaly syndromes reported in (Rivière *et al.*, 2012). Sequencing of *MTOR*, other downstream PI3K/AKT pathway members, and additional genes related to this pathway may identify further causative mutations. Accordingly, in future studies we plan to screen the mutation-negative specimens from this cohort as well as additional specimens with an extended gene panel.

PI3K/AKT pathway activation in HMEG/FCD

We used western blotting, immunohistochemistry, and *in vitro* kinase assays to look for activation of the PI3K/AKT pathway in our HMEG/FCD specimens. We found the highest levels of T308 (PI3K driven) AKT phosphorylation and AKT kinase activity in specimens with identified mutations, but also found elevated T308 AKT phosphorylation in the majority of patients with HMEG or FCD IIa/IIb, regardless of mutation status. Previous studies of AKT phosphorylation in HMEG/FCD have not examined the T308 phosphorylation site (Ljungberg *et al.*, 2006; Schick *et al.*, 2006). Although specimen LR12-251 (FCD IIa and *PIK3CA* p.His1047Arg mutation) exhibited only mildly increased levels of AKT phosphorylation on western blotting of brain homogenates, pronounced elevation of AKT kinase activity was evident in the functional kinase assay. Based on *in vitro* studies, AKT phosphorylated at both the S473 and T308 sites has up to 20-fold greater activity than AKT phosphorylated at S473 or T308 alone (Alessi *et al.*, 1996). We believe that while the small population of cells in specimen LR12-251 containing the activating p.His1047Arg PIK3CA mutation (<10%) was insufficient to cause substantially elevated levels of phospho-AKT as determined by western blotting of tissue homogenates, in individual cells with the mutation the activity of AKT phosphorylated at both S473 and T308 was sufficiently high to be detectable by the functional assay, supporting the higher sensitivity of this method.

We further hypothesize that patients with HMEG or FCD and evidence of increased PI3K/AKT/mTOR pathway activity, but negative sequencing results, either have mutations of other genes influencing the pathway, very low level mosaic mutations below the detection limit of our techniques, or aberrant activation of the pathway through other mechanisms. Elevated S473 AKT and protein S6 phosphorylation were found in all HMEG/FCD II specimens, similar to previous reports (Baybis *et al.*, 2004; Ljungberg *et al.*, 2006; Schick *et al.*, 2006, 2007; Aronica *et al.*, 2007; Sarnat *et al.*, 2012). Interestingly, we also found evidence of increased S473 phospho-AKT in epilepsy specimens without dysplasia, supporting a role for the downstream PI3K/AKT/mTOR pathway in seizures of many causes, as has been seen in rodent models (Zeng *et al.*, 2009; Berdichevsky *et al.*, 2013; Macias *et al.*, 2013) and recent human epilepsy studies (Liu *et al.*, 2014). In our immunohistochemistry studies we analysed protein S6 phosphorylation at $Ser^{235/236}$, which is mediated by the Ras/ERK signalling cascade as well as by the PI3K/AKT/mTOR pathway (Roux *et al.*, 2007), so an additional contribution of the Ras/ERK pathway to our findings cannot be ruled out.

Genotype–phenotype analysis

Our studies strongly support a single pathobiological spectrum of disease for DMEG, HMEG and FCD, but also demonstrate more heterogeneity within each category than apparent from previous studies. Although all of our HMEG and FCD type II specimens displayed cortical dyslamination and dysmorphic neurons, we found that activating mutations of different PI3K/AKT pathway core components had different effects on neuronal morphology. Mutations of *PIK3CA* were associated with only mildly enlarged neuronal size, whereas mutation of *AKT3* was associated with dramatically enlarged neuronal size. These data support previous *in vitro* experiments, in which transfection of a constitutively active form of *AKT* into cultured hippocampal neurons caused more prominent neuronal hypertrophy than transfection of a constitutively active form of *PIK3CA* (Kumar *et al.*, 2005). The same variation was seen among mutation-negative brain samples, which suggests further aetiologic heterogeneity. Studies of larger groups of specimens with identified mutations are needed to confirm these initial observations. We further predict that differences in morphology will be associated with differences in biochemical and neurophysiological phenotype, differences in the causal genes, and potentially differential sensitivity to targeted therapies.

Type 1 mosaicism

Genetic mosaicism may be classified as either type 1 or type 2 (Happle, 1997). Type 1 mosaicism is caused by heterozygous post-zygotic mutations. Our data and recent reports (Lee *et al.*, 2012; Poduri *et al.*, 2012) prove that HMEG,

and now DMEG and FCD IIa, can represent type 1 mosaicism. HMEG and FCD demonstrate most of the features previously associated with mosaicism. These include (i) nil or very low recurrence risk; (ii) asymmetric and often patchy pattern of abnormalities; (iii) variable extent of involvement; and (iv) lack of diffuse involvement (Happle, 1987). Many mosaic disorders including HMEG also have increased or decreased growth (Tinkle *et al.*, 2005). To these features we add discordant occurrence in monozygotic twins, which has been reported for FCD (Briellmann *et al.*, 2001).

The post-zygotic mutations leading to developmental disorders such as HMEG and FCD most likely occur early in embryogenesis, and the resulting phenotypes depend on the developmental timing and cell type affected as well as the gene and specific mutation. The best examples to date involve *PIK3CA*. Three activating mutations of *PIK3CA* have been identified as 'hot spots' in cancer, p.Glu542Lys, p.Glu545Lys, and p.His1047Arg (Samuels *et al.*, 2004; Zhao *et al.*, 2005). Germline expression of these mutations would likely result in embryonic lethality. Adding our data to other recent reports, post-zygotic *PIK3CA* hotspot mutations have been observed in syndromes affecting multiple tissues in large areas of the body (i.e. CLOVES syndrome), in single tissues or areas with limited extension to other tissues (i.e. HMEG with epidermal nevus), and in very localized tissues or areas (i.e. seborrheic keratoses, benign lichenoid keratoses, type 1 macrodactyly, HMEG and FCD IIa) (Hafner *et al.*, 2007; Groesser *et al.*, 2012; Kurek *et al.*, 2012; Lee *et al.*, 2012; Lindhurst *et al.*, 2012; Rios *et al.*, 2013; Keppler-Noreuil *et al.*, 2014). It follows that mosaic mutations leading to CLOVES syndrome are likely to occur very early in embryogenesis, and mutations causing the other phenotypes somewhat later. Consistent with this prediction, several patients with both CLOVES syndrome and DMEG (e.g. Patient LR12-033) or HMEG have been reported (Gucev *et al.*, 2008; Poretti *et al.*, 2013). Less severe activating mutations of *PIK3CA*, also heterozygous and mosaic but found at higher levels in more tissues, result in megalencephaly-capillary malformation syndrome with or without cortical dysplasia (Rivière *et al.*, 2012). This demonstrates that the specific mutation is also important in determining the final phenotype.

Although fewer affected individuals have been reported, a similar spectrum has been seen with mutations of *AKT3*. Germline duplication of *AKT3* has been associated with megalencephaly (Wang *et al.*, 2013). Two children with mosaic duplication of 1q (including *AKT3*) and two with the severe activating mutation p.Glu17Lys were identified in previous studies of HMEG (Lee *et al.*, 2012; Poduri *et al.*, 2012). Mosaic duplication of *AKT3* was also recently discovered in resected FCD type Ib tissue (Conti *et al.*, 2014). We found the p.Glu17Lys *AKT3* mutation in brain from a female child with left HMEG, right posterior FCD, left unilateral enlarged eye, and striking vascular malformations of the skin that resemble a severe port-wine stain with subcutaneous hypotrophy or a variant of cutis marmorata telangiectatica congenital. These extensive findings suggest earlier embryonic timing of her mutation compared to previously reported patients with mosaic p.Glu17Lys *AKT3* mutation and isolated HMEG.

Type 2 mosaicism

Our data and several previous reports also support the occurrence of type 2 mosaicism in HMEG and FCD. Type 2 mosaicism occurs when a germline heterozygous mutation is followed by a post-zygotic mutation of the other allele, resulting in a more severe condition in the affected segment (Happle, 1997; Itin and Buechner, 1999). We unexpectedly found a germline mutation of *PTEN* (p.Tyr68His) in a 9-year-old male with HMEG but no other abnormalities at the time of his last evaluation. This same mutation has been identified in individuals with PTEN hamartoma tumour syndrome (Marsh *et al.*, 1998; Pilarski *et al.*, 2011), and recombinant PTEN containing this mutation demonstrates defective phosphatase activity (Han *et al.*, 2000). HMEG and FCD have not been described in large series of patients with *PTEN* mutations (Eng, 2003; Pilarski *et al.*, 2011, 2013). However, rare reports have appeared of germline mutations of *PTEN* associated with HMEG (Merks *et al.*, 2003) or FCD (Elia *et al.*, 2012; O'Rourke *et al.*, 2012; Child and Cascino, 2013), including one remarkable example of a mosaic mutation of *PTEN* in dysplastic neurons in FCD IIb, but not in nearby normal neurons or blood-derived DNA (Schick *et al.*, 2006). We hypothesize that all of these children have type 2 mosaicism, with a second hit in the other *PTEN* allele or possibly another gene affecting the PI3K/AKT pathway. Type 2 mosaicism for *PTEN* has been reported in other segmental overgrowth syndromes (Caux *et al.*, 2007). Mice with heterozygous loss of *PTEN* in brain have no apparent phenotype, whereas those with homozygous *PTEN* loss exhibit neuronal hypertrophy and seizures (Backman *et al.*, 2001; Kwon *et al.*, 2001; Ljungberg *et al.*, 2009). These findings, in concert with our identification of cellular hypertrophy and elevated protein S6 and T308 AKT phosphorylation in only a subset of neurons in cortex from our germline heterozygous *PTEN* mutation subject, support the hypothesis that a second mosaic mutation is necessary to cause cortical dysplasia.

Summary and implications

In this study, we present diverse data from brain imaging, histopathology, immunohistochemistry and deep sequencing of a large cohort of children with dysplastic cortical malformations. Our results show that MEG, HMEG and FCD comprise a complete series of overlapping phenotypes associated with upregulation of the PI3K/AKT/mTOR pathway, as shown in Fig. 7. We accordingly propose that they be classified as a single malformation of cortical

development with variable expressivity rather than as separate disorders.

In the genetics literature, mosaic phenotypes localized to an anatomically recognizable portion of the body are designated as segmental mosaicism (Happle, 1997; Youssoufian and Pyeritz, 2002; Biesecker and Spinner, 2013). Respecting this usage, we have begun using the term PI3K/AKT-associated segmental cortical dysplasia to refer to the complete spectrum, with DMEG, HMEG and FCD used as anatomic subsets when clinically relevant. A thorough classification scheme of these segmental dysplasias would incorporate the distribution of the malformation as determined by brain imaging (bihemispheric symmetric, bihemispheric asymmetric, hemispheric, multilobar, or intralobar), the histopathology (FCD type Ia–c, IIa–b, or IIIa–d) (Blumcke *et al.*, 2011), and the identified aetiology. As an example, for our Patient LR11-443, the nomenclature would be 'bihemispheric asymmetric cortical dysplasia, histologic type IIa, due to mosaic *AKT3* p.Glu17Lys mutation'. This classification could then evolve as new causative mechanisms for dysplastic brain malformations are identified.

Multiple selective inhibitors of PI3K and AKT are currently in clinical trials for treatment of cancer (Bellacosa *et al.*, 2005; Engelman, 2009; Willems *et al.*, 2012). It is tempting to hypothesize that these agents may be useful in the management of epilepsy and associated conditions in the segmental cortical dysplasia spectrum, similar to what has been suggested for the use of mTOR inhibitors in tuberous sclerosis (Krueger *et al.*, 2013; Wiegand *et al.*, 2013; Cardamone *et al.*, 2014). Testing of these compounds in mouse and *in vitro* models of abnormal neuronal PI3K/AKT pathway activation will be an important first step in evaluating the possible benefits of these compounds for treatment of children with dysplastic brain malformations.

Acknowledgements

The authors thank the study patients and their families, without whose participation this work would not be possible, and the Seattle Children's Hospital Epilepsy Program team.

Funding

Research reported in this publication was supported by the National Institute of Neurological Disorders and Stroke (NINDS) of the National Institutes of Health (NIH) under award numbers K02NS072162 to L.A.J. and R01NS058721 to W.B.D., and by the National Cancer Institute (NCI) of the NIH under award number CA160080 to J.S.

Supplementary material

Supplementary material is available at *Brain* online.

References

Alessi DR, Andjelkovic M, Caudwell B, Cron P, Morrice N, Cohen P, et al. Mechanism of activation of protein kinase B by insulin and IGF-1. EMBO J 1996; 15: 6541–51.

Arch EM, Goodman BK, Van Wesep RA, Liaw D, Clarke K, Parsons R, et al. Deletion of PTEN in a patient with Bannayan-Riley-Ruvalcaba syndrome suggests allelism with Cowden disease. Am J Med Genet 1997; 71: 489–93.

Aronica E, Boer K, Baybis M, Yu J, Crino P. Co-expression of cyclin D1 and phosphorylated ribosomal S6 proteins in hemimegalencephaly. Acta Neuropathol (Berl) 2007; 114: 287–93.

Backman SA, Stambolic V, Suzuki A, Haight J, Elia A, Pretorius J, et al. Deletion of Pten in mouse brain causes seizures, ataxia and defects in soma size resembling Lhermitte-Duclos disease. Nat Genet 2001; 29: 396–403.

Barkovich AJ, Chuang SH. Unilateral megalencephaly: correlation of MR imaging and pathologic characteristics. Am J Neuroradiol 1990; 11: 523–31.

Baybis M, Yu J, Lee A, Golden JA, Weiner H, McKhann G, et al. mTOR cascade activation distinguishes tubers from focal cortical dysplasia. Ann Neurol 2004; 56: 478–87.

Bellacosa A, Kumar CC, Di Cristofano A, Testa JR. Activation of AKT kinases in cancer: implications for therapeutic targeting. Adv Cancer Res 2005; 94: 29–86.

Berdichevsky Y, Dryer AM, Saponjian Y, Mahoney MM, Pimentel CA, Lucini CA, et al. PI3K-Akt signaling activates mTOR-mediated epileptogenesis in organotypic hippocampal culture model of post-traumatic epilepsy. J Neurosci 2013; 33: 9056–67.

Bhaskar PT, Hay N. The Two TORCs and Akt. Dev. Cell 2007; 12: 487–502.

Biesecker LG, Spinner NB. A genomic view of mosaicism and human disease. Nat Rev Genet 2013; 14: 307–20.

Blumcke I, Thom M, Aronica E, Armstrong DD, Vinters HV, Palmini A, et al. The clinicopathologic spectrum of focal cortical dysplasias: a consensus classification proposed by an ad hoc Task Force of the ILAE Diagnostic Methods Commission. Epilepsia 2011; 52: 158–74.

Bonneau D, Longy M. Mutations of the human PTEN gene. Hum Mutat 2000; 16: 109–22.

Briellmann RS, Jackson GD, Torn-Broers Y, Berkovic SF. Causes of epilepsies: insights from discordant monozygous twins. Ann Neurol 2001; 49: 45–52.

Cardamone M, Flanagan D, Mowat D, Kennedy SE, Chopra M, Lawson JA. Mammalian target of rapamycin inhibitors for intractable epilepsy and subependymal giant cell astrocytomas in tuberous sclerosis complex. J Pediatr 2014; 164: 1195–200.

Caux F, Plauchu H, Chibon F, Faivre L, Fain O, Vabres P, et al. Segmental overgrowth, lipomatosis, arteriovenous malformation and epidermal nevus (SOLAMEN) syndrome is related to mosaic PTEN nullizygosity. Eur J Hum Genet 2007; 15: 767–73.

Child ND, Cascino GD. Mystery case: Cowden syndrome presenting with partial epilepsy related to focal cortical dysplasia. Neurology 2013; 81: e98–99.

Colombo N, Tassi L, Deleo F, Citterio A, Bramerio M, Mai R, et al. Focal cortical dysplasia type IIa and IIb: MRI aspects in 118 cases proven by histopathology. Neuroradiology 2012; 54: 1065–77.

Conti V, Pantaleo M, Barba C, Baroni G, Mei D, Buccoliero AM, et al. Focal dysplasia of the cerebral cortex and infantile spasms associated with somatic 1q21.1-q44 duplication including the AKT3 gene. Clin Genet 2014. Advance Access published on August 5, 2014, doi: 10.1111/cge.12476.

Elia M, Amato C, Bottitta M, Grillo L, Calabrese G, Esposito M, et al. An atypical patient with Cowden syndrome and PTEN gene mutation presenting with cortical malformation and focal epilepsy. Brain Dev 2012; 34: 873–6.

Eng C. PTEN: one gene, many syndromes. Hum Mutat 2003; 22: 183–98.
Engelman JA. Targeting PI3K signalling in cancer: opportunities, challenges and limitations. Nat Rev Cancer 2009; 9: 550–62.
European Chromosome 16 Tuberous Sclerosis Consortium. Identification and characterization of the tuberous sclerosis gene on chromosome 16. Cell 1993; 75: 1305–15.
Fauser S, Sisodiya SM, Martinian L, Thom M, Gumbinger C, Huppertz H-J, et al. Multi-focal occurrence of cortical dysplasia in epilepsy patients. Brain J Neurol 2009; 132: 2079–90.
Flores-Sarnat L. Hemimegalencephaly: part 1. Genetic, clinical, and imaging aspects. J Child Neurol 2002; 17: 373–84discussion 384.
Groesser L, Herschberger E, Landthaler M, Hafner C. FGFR3, PIK3CA and RAS mutations in benign lichenoid keratosis. Br J Dermatol 2012; 166: 784–8.
Gucev ZS, Tasic V, Jancevska A, Konstantinova MK, Pop-Jordanova N, Trajkovski Z, et al. Congenital lipomatous overgrowth, vascular malformations, and epidermal nevi (CLOVE) syndrome: CNS malformations and seizures may be a component of this disorder. Am J Med Genet A 2008; 146A: 2688–90.
Hafner C, López-Knowles E, Luis NM, Toll A, Baselga E, Fernández-Casado A, et al. Oncogenic PIK3CA mutations occur in epidermal nevi and seborrheic keratoses with a characteristic mutation pattern. Proc Natl Acad Sci USA 2007; 104: 13450–4.
Han SY, Kato H, Kato S, Suzuki T, Shibata H, Ishii S, et al. Functional evaluation of PTEN Missense mutations using *in vitro* phosphoinositide phosphatase assay. Cancer Res 2000; 60: 3147–51.
Happle R. Lethal genes surviving by mosaicism: a possible explanation for sporadic birth defects involving the skin. J Am Acad Dermatol 1987; 16: 899–906.
Happle R. A rule concerning the segmental manifestation of autosomal dominant skin disorders. Review of clinical examples providing evidence for dichotomous types of severity. Arch Dermatol 1997; 133: 1505–9.
Hauptman JS, Mathern GW. Surgical treatment of epilepsy associated with cortical dysplasia: 2012 update. Epilepsia 2012; 53 (Suppl 4): 98–104.
Hiatt JB, Pritchard CC, Salipante SJ, O'Roak BJ, Shendure J. Single molecule molecular inversion probes for targeted, high-accuracy detection of low-frequency variation. Genome Res 2013; 23: 843–54.
Huttenlocher PR, Wollmann RL. Cellular neuropathology of tuberous sclerosis. Ann N Y Acad Sci 1991; 615: 140–8.
Itin PH, Buechner SA. Segmental forms of autosomal dominant skin disorders: the puzzle of mosaicism. Am J Med Genet 1999; 85: 351–4.
Jahan R, Mischel PS, Curran JG, Peacock WJ, Shields DW, Vinters HV. Bilateral neuropathologic changes in a child with hemimegalencephaly. Pediatr Neurol 1997; 17: 344–9.
Keppler-Noreuil KM, Sapp JC, Lindhurst MJ, Parker VER, Blumhorst C, Darling T, et al. Clinical delineation and natural history of the PIK3CA-related overgrowth spectrum. Am J Med Genet A 2014; 164: 1713–33.
Kometani H, Sugai K, Saito Y, Nakagawa E, Sakuma H, Komaki H, et al. Postnatal evolution of cortical malformation in the 'non-affected' hemisphere of hemimegalencephaly. Brain Dev 2010; 32: 412–16.
Krueger DA, Wilfong AA, Holland-Bouley K, Anderson AE, Agricola K, Tudor C, et al. Everolimus treatment of refractory epilepsy in tuberous sclerosis complex. Ann Neurol 2013; 74: 679–87.
Kumar V, Zhang M-X, Swank MW, Kunz J, Wu G-Y. Regulation of dendritic morphogenesis by Ras-PI3K-Akt-mTOR and Ras-MAPK signaling pathways. J Neurosci 2005; 25: 11288–99.
Kurek KC, Luks VL, Ayturk UM, Alomari AI, Fishman SJ, Spencer SA, et al. Somatic mosaic activating mutations in PIK3CA cause CLOVES syndrome. Am J Hum Genet 2012; 90: 1108–15.
Kwon CH, Zhu X, Zhang J, Knoop LL, Tharp R, Smeyne RJ, et al. Pten regulates neuronal soma size: a mouse model of Lhermitte-Duclos disease. Nat Genet 2001; 29: 404–11.
Lee JH, Huynh M, Silhavy JL, Kim S, Dixon-Salazar T, Heiberg A, et al. De novo somatic mutations in components of the PI3K-AKT3-mTOR pathway cause hemimegalencephaly. Nat Genet 2012; 44: 941–5.
Liaw D, Marsh DJ, Li J, Dahia PL, Wang SI, Zheng Z, et al. Germline mutations of the PTEN gene in Cowden disease, an inherited breast and thyroid cancer syndrome. Nat Genet 1997; 16: 64–7.
Lindhurst MJ, Parker VER, Payne F, Sapp JC, Rudge S, Harris J, et al. Mosaic overgrowth with fibroadipose hyperplasia is caused by somatic activating mutations in PIK3CA. Nat Genet 2012; 44: 928–33.
Liu J, Reeves C, Michalak Z, Coppola A, Diehl B, Sisodiya SM, et al. Evidence for mTOR pathway activation in a spectrum of epilepsy-associated pathologies. Acta Neuropathol Commun 2014; 2: 71.
Ljungberg MC, Bhattacharjee MB, Lu Y, Armstrong DL, Yoshor D, Swann JW, et al. Activation of mammalian target of rapamycin in cytomegalic neurons of human cortical dysplasia. Ann Neurol 2006; 60: 420–9.
Ljungberg MC, Sunnen CN, Lugo JN, Anderson AE, D'Arcangelo G. Rapamycin suppresses seizures and neuronal hypertrophy in a mouse model of cortical dysplasia. Dis Model Mech 2009; 2: 389–98.
Macias M, Blazejczyk M, Kazmierska P, Caban B, Skalecka A, Tarkowski B, et al. Spatiotemporal characterization of mTOR kinase activity following kainic acid induced status epilepticus and analysis of rat brain response to chronic rapamycin treatment. PloS One 2013; 8: e64455.
Manning BD, Cantley LC. AKT/PKB signaling: navigating downstream. Cell 2007; 129: 1261–74.
Marsh DJ, Coulon V, Lunetta KL, Rocca-Serra P, Dahia PL, Zheng Z, et al. Mutation spectrum and genotype-phenotype analyses in Cowden disease and Bannayan-Zonana syndrome, two hamartoma syndromes with germline PTEN mutation. Hum Mol Genet 1998; 7: 507–15.
Merks JHM, De Vries LS, Zhou XP, Nikkels P, Barth PG, Eng C, et al. PTEN hamartoma tumour syndrome: variability of an entity. J Med Genet 2003; 40: e111.
Mirzaa GM, Parry DA, Fry AE, Giamanco KA, Schwartzentruber J, Vanstone M, et al. *De novo* CCND2 mutations leading to stabilization of cyclin D2 cause megalencephaly-polymicrogyria-polydactyly-hydrocephalus syndrome. Nat Genet 2014; 46: 510–5.
Nakahashi M, Sato N, Yagishita A, Ota M, Saito Y, Sugai K, et al. Clinical and imaging characteristics of localized megalencephaly: a retrospective comparison of diffuse hemimegalencephaly and multilobar cortical dysplasia. Neuroradiology 2009; 51: 821–30.
O'Roak BJ, Vives L, Fu W, Egertson JD, Stanaway IB, Phelps IG, et al. Multiplex targeted sequencing identifies recurrently mutated genes in autism spectrum disorders. Science 2012; 338: 1619–22.
O'Rourke DJ, Twomey E, Lynch S-A, King MD. Cortical dysplasia associated with the PTEN mutation in Bannayan Riley Ruvalcaba syndrome: a rare finding. Clin Dysmorphol 2012; 21: 91–2.
Pilarski R, Burt R, Kohlman W, Pho L, Shannon KM, Swisher E. Cowden syndrome and the PTEN hamartoma tumor syndrome: systematic review and revised diagnostic criteria. J Natl Cancer Inst 2013; 105: 1607–16.
Pilarski R, Stephens JA, Noss R, Fisher JL, Prior TW. Predicting PTEN mutations: an evaluation of Cowden syndrome and Bannayan–Riley–Ruvalcaba syndrome clinical features. J Med Genet 2011; 48: 505–12.
Poduri A, Evrony GD, Cai X, Elhosary PC, Beroukhim R, Lehtinen MK, et al. Somatic activation of AKT3 causes hemispheric developmental brain malformations. Neuron 2012; 74: 41–8.
Poretti A, Meoded A, Rossi A, Raybaud C, Huisman TAGM. Diffusion tensor imaging and fiber tractography in brain malformations. Pediatr Radiol 2013; 43: 28–54.

Richardson EP Jr. Pathology of tuberous sclerosis. Neuropathologic aspects. Ann N Y Acad Sci 1991; 615: 128–39.

Rios JJ, Paria N, Burns DK, Israel BA, Cornelia R, Wise CA, et al. Somatic gain-of-function mutations in PIK3CA in patients with macrodactyly. Hum Mol Genet 2013; 22: 444–51.

Rivière JB, Mirzaa GM, O'Roak BJ, Beddaoui M, Alcantara D, Conway RL, et al. *De novo* germline and postzygotic mutations in AKT3, PIK3R2 and PIK3CA cause a spectrum of related megalencephaly syndromes. Nat Genet 2012; 44: 934–40.

Roux PP, Shahbazian D, Vu H, Holz MK, Cohen MS, Taunton J, et al. RAS/ERK signaling promotes site-specific ribosomal protein S6 phosphorylation via RSK and stimulates cap-dependent translation. J Biol Chem 2007; 282: 14056–64.

Samuels Y, Wang Z, Bardelli A, Silliman N, Ptak J, Szabo S, et al. High frequency of mutations of the PIK3CA gene in human cancers. Science 2004; 304: 554.

Sarnat H, Flores-Sarnat L, Crino P, Hader W, Bello-Espinosa L. Hemimegalencephaly: foetal tauopathy with mTOR hyperactivation and neuronal lipidosis. Folia Neuropathol 2012; 50: 330–45.

Schick V, Majores M, Engels G, Hartmann W, Elger CE, Schramm J, et al. Differential Pi3K-pathway activation in cortical tubers and focal cortical dysplasias with balloon cells. Brain Pathol 2007; 17: 165–73.

Schick V, Majores M, Engels G, Spitoni S, Koch A, Elger CE, et al. Activation of Akt independent of PTEN and CTMP tumor-suppressor gene mutations in epilepsy-associated Taylor-type focal cortical dysplasias. Acta Neuropathol (Berl) 2006; 112: 715–25.

Slegtenhorst M van, Hoogt R de, Hermans C, Nellist M, Janssen B, Verhoef S, et al. Identification of the tuberous sclerosis gene TSC1 on chromosome 9q34. Science 1997; 277: 805–8.

Tinkle BT, Schorry EK, Franz DN, Crone KR, Saal HM. Epidemiology of hemimegalencephaly: a case series and review. Am J Med Genet A 2005; 139: 204–11.

Wang D, Zeesman S, Tarnopolsky MA, Nowaczyk M. Duplication of AKT3 as a cause of macrocephaly in duplication 1q43q44. Am J Med Genet A 2013; 161: 2016–19.

Wiegand G, May TW, Ostertag P, Boor R, Stephani U, Franz DN. Everolimus in tuberous sclerosis patients with intractable epilepsy: a treatment option? Eur J Paediatr Neurol 2013; 17: 631–8.

Willems L, Tamburini J, Chapuis N, Lacombe C, Mayeux P, Bouscary D. PI3K and mTOR Signaling pathways in cancer: new data on targeted therapies. Curr Oncol Rep 2012; 14: 129–38.

Youssoufian H, Pyeritz RE. Mechanisms and consequences of somatic mosaicism in humans. Nat Rev Genet 2002; 3: 748–58.

Zeng LH, Rensing NR, Wong M. The mammalian target of rapamycin signaling pathway mediates epileptogenesis in a model of temporal lobe epilepsy. J Neurosci 2009; 29: 6964–72.

Zhao JJ, Liu Z, Wang L, Shin E, Loda MF, Roberts TM. The oncogenic properties of mutant p110α and p110β phosphatidylinositol 3-kinases in human mammary epithelial cells. Proc Natl Acad Sci USA 2005; 102: 18443–8.